THE ASTROPHYSICAL JOURNAL, 413:582–592, 1993 August 20

COMPACT AMMONIA SOURCES TOWARD THE G10.5+0.0 H II REGION COMPLEX

GUIDO GARAY,[1] JAMES M. MORAN,[2] AND LUIS F. RODRÍGUEZ[3]

Received 1992 July 27; accepted 1993 February 24

ABSTRACT

We present observations of the (2, 2) and (3, 3) inversion transitions of ammonia toward a group of compact H II regions near $l = 10.^{\circ}5$, $b = 0.^{\circ}0$, made at 4″ resolution using the VLA. We detected three distinct ammonia sources in a region of ~2′ in diameter. The densest and hottest cloud, having a line center velocity of 66.9 ± 0.2 km s^{-1}, is associated with the G10.47+0.03 cluster of ultracompact H II regions. It exhibits a core-halo structure, with a core of ~0.08 pc in size surrounded by an envelope of ~0.25 pc in diameter. The peak optical depth in the main line of the (2, 2) and (3, 3) transitions are 25 and 37, respectively. The rotational temperature of the ammonia gas rises from ~25 K in the outer parts of the halo to ~75 K at the center of the core. The ammonia column density rises from $\sim 4 \times 10^{17}$ cm^{-2} in the envelope region to $\sim 4 \times 10^{18}$ cm^{-2} in the central position. The NH_3 emission from the core region is remarkably broad in velocity; the line widths of the (2, 2) and (3, 3) main lines are 12.2 ± 1.2 and 11.6 ± 0.5 km s^{-1}, respectively. The observed velocity structure of the ammonia emission indicates that the halo is slowly rotating, with an angular velocity of 9.5 ± 1.1 km s^{-1} pc^{-1}, while the gas in the core is undergoing rapid motions. A second cloud, having an angular size of ~13″, a line center velocity of 71.3 ± 0.2 km s^{-1}, and a line width of 3.5 km s^{-1}, is found toward the G10.46+0.03 complex region of ionized gas. It has a rotational temperature of 48 ± 6 K and an NH_3 column density of $\sim 1 \times 10^{16}$ cm^{-2}. The velocity structure of the ammonia emission suggests that this cloud is probably expanding, with a velocity of ~2 km s^{-1}. The third cloud, at $l = 10.^{\circ}48$, $b = 0.^{\circ}03$, has a size of ~9″, a line center velocity of 65.4 ± 0.9 km s^{-1}, and a line width of 3.5 km s^{-1}, and is not associated with any known radio continuum emission. It may represent a molecular core undergoing gravitational collapse in a stage prior to the formation of a star.

Subject headings: H II regions — ISM: individual (G10.5+0.0) — ISM: kinematics and dynamics — ISM: molecules

1. INTRODUCTION

Aperture synthesis radio continuum observations have shown the presence of several sources toward the $l = 10.^{\circ}5$, $b = 0.^{\circ}0$ Galactic direction. At angular resolutions of ~15″, G10.5+0.0 consists of three extended, complex sources spread over a region of ~3′ in diameter (Garay et al. 1993). Two of these complexes, G10.46+0.03 and G10.47+0.03, contain ultracompact H II regions indicating that they are the sites of recent formation of massive stars (Wood & Churchwell 1989; Garay et al. 1993). Other signs of active star formation, such as H_2O maser emission (Genzel & Downes 1977; Churchwell, Walmsley, & Cesaroni 1990) and OH maser emission (Braz & Sivagnanam 1987), are also present toward this region.

Ultracompact H II regions are thought to indicate the first stage of the evolution of newly formed massive stars still embedded in their natal molecular gas. Since they are most likely ionization-bounded, they should be surrounded by neutral matter that is being heated and excited by the stellar luminosity from the central source. High angular resolution observations of ammonia toward regions forming massive stars have in fact shown the presence of dense and warm cores of molecular gas associated with bright and small regions of ionized gas (Keto, Ho, & Haschick 1987a; Keto, Ho, & Reid 1987b; Garay & Rodríguez 1990). The ammonia emission most probably originates in the warm, high-density molecular gas close to the embedded O star. Molecular cores are thus thought to be part of the remnant gas from which the OB stars formed, and therefore they are useful objects for studying the physical conditions and dynamics of the gas in the earliest stages of star formation.

Molecular line observations toward the G10.5+0.0 region, made with the Effelsberg 100 m telescope (HPBW of 40″), have shown strong emission in the main and satellite hyperfine (HF) lines of several inversion transitions of NH_3 (Churchwell et al. 1990; Cesaroni, Walmsley, & Churchwell 1992) and in several rotational lines of $C^{34}S$ (Cesaroni et al. 1991). The lines are unusually broad, with a FWHM velocity width of ~8 km s^{-1}. Cesaroni et al. (1992) concluded that the ammonia spectra are best fitted by a two-component model consisting of a highly optically thick clump, responsible for the strong emission in the satellite lines, plus a component of lower optical depth that contributes only to the main line. These observations, however, did not have the angular resolution to determine the location of the molecular emission with respect to the compact H II regions, nor to resolve its spatial structure.

We report here observations of the (2, 2) and (3, 3) inversion transitions of NH_3 made with the VLA, at an angular resolution of 4″, toward the $l = 10.^{\circ}5$, $b = 0.^{\circ}0$ Galactic region. These lines are probes of warm ($T \geq 50$ K) and dense [$n(H_2) \geq 10^4$ cm^{-3}] molecular gas. The purpose of these observations was to find out where the dense NH_3 gas resides with respect to the compact H II regions, to determine its morphology and velocity structure, and to investigate the physical conditions within the ammonia clouds.

[1] Departamento de Astronomía, Universidad de Chile, Casilla 36-D, Santiago, Chile.
[2] Harvard-Smithsonian Center for Astrophysics, 60 Garden Street, MS 42, Cambridge, MA 02138.
[3] Instituto de Astronomía, UNAM, Apdo. Postal 70-264, 04510 México, D.F., Mexico.

2. OBSERVATIONS

The observations were made with the Very Large Array of the National Radio Astronomy Observatory.[4] The array was in the D configuration, which provides a range of spacings from 40 to 1000 m. This range of spacings makes structures larger than about 60″ undetectable at 1.3 cm. The phase center of the array was set at $\alpha(1950) = 18^h05^m39^s.0$ and $\delta(1950) = -12°52'30''.0$.

We observed the $(J, K) = (3, 3)$ inversion transition of ammonia on 1988 September 19, and the $(J, K) = (2, 2)$ inversion transition on 1988 September 21. We assumed rest frequencies of 23722.633 for the (2, 2) transition and 23870.129 MHz for the (3, 3) transition. We used a bandpass of 12.5 MHz, centered at an LSR velocity of 53.3 km s^{-1}, and 63 spectral channels 195.3 KHz wide each (about 2.5 km s^{-1} at the observing frequencies). The integration time on source was ~60 minutes for both the (2, 2) and the (3, 3) transitions, with 25 antennas. Each 10 minute scan on source was paired with a 3 minute calibration scan on the source 1730−130. The data were edited and calibrated by applying the complex gain solution from the calibration source. The flux density scale was determined by observing 3C 286 for which we assumed a flux density of 2.4 Jy at 1.3 cm. The bandpass response was normalized using the observations of the calibrators 3C 273 and 1730−130.

The *u,v* data were Fourier transformed and cleaned using the MX algorithm. We used a Gaussian taper of 40 $k\lambda$ in order to increase the sensitivity to low surface brightness emission. The synthesized beams were 4″.7 × 3″.6 and 5″.3 × 3″.8 at the frequencies of the (2, 2) and (3, 3) lines, respectively. The rms noise level in a single spectral line channel was 59 and 32 mJy per beam solid angle for the (2, 2) and (3, 3) observations, respectively. To convert to brightness temperature, the fluxes per beam in mJy should be multiplied by 0.13 for the (2, 2) observations and 0.11 for the (3, 3) observations. Line maps were made from the individual channel maps by subtracting a continuum map made from the average of all line-free channel maps.

3. RESULTS

3.1. *Continuum Map*

Figure 1 shows the 23.9 GHz radio continuum map toward the $l = 10°.5$, $b = 0°.0$ Galactic direction made using the average of off-line channel maps from the (3, 3) observations. It shows two main sources: a bright and compact object to the east, having a total flux density of 0.38 ± 0.03 Jy and a deconvolved angular size of 2″.2 × 1″.6; and a more extended, less bright object, ~45″ to the southwest of the former. The crosses indicate the position of the ultracompact H II regions detected at 4.9 GHz by Wood & Churchwell (1989, hereafter WC).

The eastern source corresponds to the G10.47+0.03 Galactic H II region. The three compact components detected by WC (A, B, and C) appear blended in Figure 1 due to the smaller angular resolution of our observations. Figure 2 shows the radio continuum flux density of sources A and B added together versus frequency, collected from the measurements of WC, Garay et al. (1993, hereafter GRMC), and this paper. Most of the flux density at the higher frequencies arises from

[4] The National Radio Astronomy Observatory is operated by Associated Universities, Inc., under cooperative agreement with the National Science Foundation.

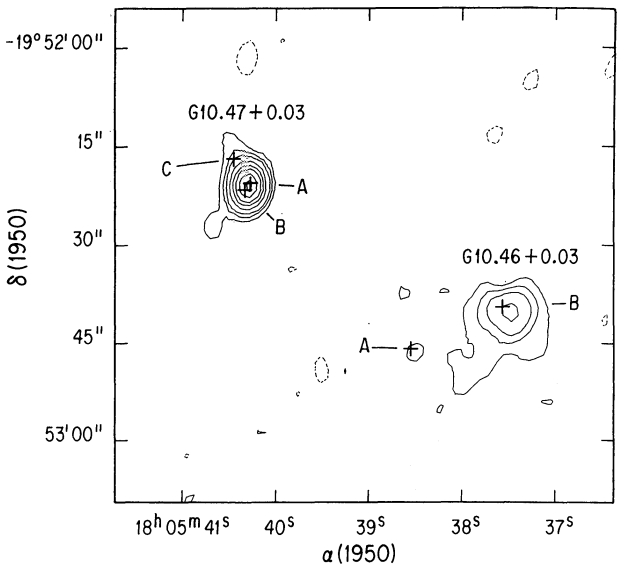

FIG. 1.—VLA continuum map toward the G10.5+0.0 Galactic region at 23.9 GHz with 5″.3 × 3″.8 resolution. Contour levels are {−1, 1, 2, 3, 5, 7, 9, 12, and 15} × 20 mJy per beam. The crosses mark the position of the ultracompact H II regions detected by Wood & Churchwell (1989).

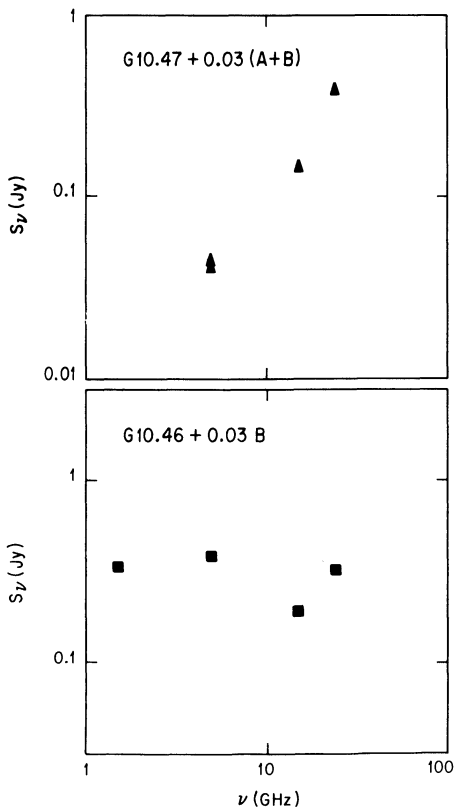

FIG. 2.—Plot of radio continuum flux density vs. frequency for radio sources in the $l = 10°.5$, $b = 0°.0$ region. *Top*: spectrum, between 5 and 24 GHz, of sources G10.47+0.03A and B added together. *Bottom*: spectrum, between 1.5 and 24 GHz, of the cometary H II region G10.46+0.03B.

component A of WC, which is the brightest ($T_b \sim 6000$ K) object at 4.9 GHz. The spectral index between 4.9 and 23.9 GHz is 1.7 ± 0.3. This value is consistent, within the observational errors, with that of an optically thick, uniform density H II region. We note that in the map made using the continuum channel of the (3, 3) data, G10.47+0.03 exhibits a weak elongated structure at a position angle of $\sim 35°$ west of north. A much larger structure, at roughly the same position angle, is present in the 1.5 GHz map of GRMC.

The main western continuum source corresponds to the cometary-shaped H II region G10.46+0.03B detected by GRMC at 1.5, 4.9, and 15.0 GHz. At 23.9 GHz we measured a flux density of 0.32 ± 0.03 Jy and a deconvolved size of 7".6 × 5".3. Figure 2 shows its radio continuum spectrum derived from the measurements of GRMC and this paper. The spectrum is consistent with the radio emission being free-free radiation arising from an optically thin H II region. The low value at 15.0 GHz is most likely due to the relatively high angular resolution ($\sim 3''$) used in making that measurement, which resolved out part of the emission from this extended source. Assuming an electron temperature of 10^4 K and a distance of 5.8 kpc (Churchwell et al. 1990), we derive an electron density of 4×10^3 cm^{-3}. The number of ionizing photons per second needed to account for the observed radio continuum emission is 1.1×10^{48} s^{-1}, which requires the equivalent of an O9 ZAMS exciting star. We also detected emission from G10.46+0.03A, a compact and weak source, located about 15" east of the cometary region, which was previously detected at 4.9 GHz by WC and at 4.9 and 15.0 GHz by GRMC. At 23.9 GHz we measured a flux density of ~25 mJy.

3.2. *Line Profiles and Maps*

Each energy level of an inversion doublet of NH_3 is split, due to the hyperfine interaction of the electric quadrupole moment of the N nucleus with the electric field of the electrons, into three sublevels producing a characteristic inversion spectrum consisting of a central main line and two pairs of satellite lines symmetrically placed about the main line. In the absence of non-LTE effects and in the optically thin limit, the satellite lines should have an intensity of ~5% and ~3% of that in the main line for the (2, 2) and (3, 3) transitions, respectively.

Figure 3 shows two line maps of the NH_3(3, 3) emission toward the $l = 10°.5$, $b = 0°.0$ Galactic direction. The upper panel shows the average of the line maps at the velocities of 63.1 and 65.6 km s^{-1}; the bottom panel shows the average of those at the velocities of 70.5 and 72.9 km s^{-1}. These ammonia maps reveal the presence of three remarkable molecular structures: a bright source, NH_3 G10.47+0.03, seen in both line maps; a source toward the southwest, NH_3 G10.46+0.03, evident in the higher velocity map; and a northern cloud, NH_3 G10.48+0.03, detected in the lower velocity map. In the remaining of this section we present the observational results for each of these sources. The coordinates and sizes of the ammonia clouds are given in Table 1. The observed parameters on the NH_3 line emission are summarized in Table 2.

3.2.1. NH_3 *G10.47+0.03*

This cloud is closely associated with the radio continuum source G10.47+0.03. As indicated by the crosses in Figure 3, which mark the position of the ultracompact H II regions, the two brightest ultracompact H II regions lie at the peak position of the ammonia emission. Among the three compact molecular clouds detected in the present study, NH_3 G10.47+0.03 is the one that exhibits the strongest ammonia emission. In the (3, 3) main HF line, we measured a peak beam-averaged brightness temperature of 69 K.

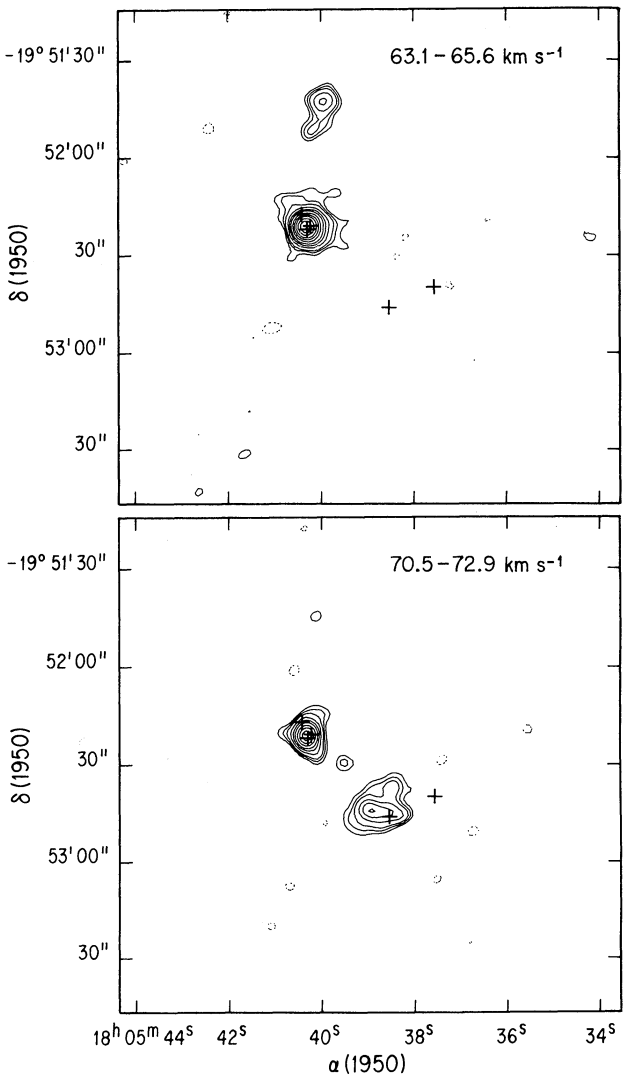

FIG. 3.—Line maps of the (3, 3) ammonia emission toward the $l = 10°.5$, $b = 0°.0$ region at 6".0 × 6".0 resolution. Contour levels are {−3, 3, 4, 5, 7, 9, 11, 14, 17, 20, 24, and 28} × 25 mJy per beam. *Top*: average of the 63.1 and 65.6 km s^{-1} line channel maps. *Bottom*: average of the 70.5 and 72.9 km s^{-1} line channel maps.

The line profiles of the (2, 2) and (3, 3) inversion lines of ammonia over an 13".2 × 13".2 region covering this source are shown in Figure 4. The pixel size is 1".2. The main and satellite

TABLE 2

AMMONIA CLOUDS

CLOUD	COORDINATES α(1950)	COORDINATES δ(1950)	ANGULAR SIZE
G10.46+0.03	18h05m38s.78	−19°52'43".5	16".0 × 10".5
G10.47+0.03	18 05 40.32	−19 52 20.9	10.2 × 7.8[a]
			3.9 × 2.3[b]
G10.48+0.03	18 05 39.97	−19 51 44.3	13.8 × 5.5

[a] Halo.
[b] Core.

TABLE 2

AMMONIA LINE PARAMETERS

Transition	V (km s^{-1})	Δv (km s^{-1})	Flux Density (Jy)
A. G10.47+0.03 Whole			
(2, 2; m)	66.8 ± 0.3	8.2 ± 0.6	1.83 ± 0.12
(3, 3; m)	66.9 ± 0.1	8.8 ± 0.4	2.72 ± 0.09
B. G10.47+0.03 Core			
(2, 2; m)	66.6 ± 0.4	12.2 ± 1.2	0.35 ± 0.03
(2, 2; s)		8.1 ± 0.9	0.25 ± 0.03
(3, 3; m)	66.7 ± 0.2	11.6 ± 0.5	0.56 ± 0.02
(3, 3; s)		9.0 ± 2.1	0.29 ± 0.04
C. G10.46+0.03			
(2, 2; m)	71.2 ± 0.3	3.4 ± 0.7	1.82 ± 0.29
(2, 2; s)			<0.087
(3, 3; m)	71.4 ± 0.2	3.6 ± 0.7	1.78 ± 0.23
(3, 3; s)			<0.042
D. G10.48+0.03			
(2, 2; m)	66.0 ± 0.5	3.3 ± 0.9	0.9 ± 0.21
(2, 2; s)	...	...	<0.087
(3, 3; m)	64.7 ± 0.2	3.6 ± 0.8	0.86 ± 0.15
(3, 3; s)	...	...	<0.042

HF lines of the (2, 2) and (3, 3) transitions are detected in emission throughout the whole source. The strong intensity of the satellite lines [at ±21.5 and ±28.9 km s^{-1} from the main line for the (3, 3) transition; and at ±16.6 and ±25.8 km s^{-1} for the (2, 2) transition], indicates that these lines have significant optical depths.

Individual line channel maps of the emission in the (3, 3) inversion transition of NH_3 in the velocity range from 28.8 to 107.3 km s^{-1}, are shown in Figure 5. The channel width is 2.45 km s^{-1}. The emission from the central line maps (velocities from 60.7 to 72.9 km s^{-1}) which cover the range of velocities of the main HF line, arises from a region of ~9″ in size. The emission from the outer channel maps, which sample the emission from the satellite HF lines, arises from a smaller region with a deconvolved size of ~3″. The most striking results from these maps are the strong emission seen in all four HF satellite lines, indicated by their F′ → F values, and the difference in the size of the main and satellite line-emitting regions.

The average radial velocity of the ammonia gas, determined by simultaneously fitting Gaussian profiles to all five quadrupole HF components, with fixed velocity separations, to the spectra obtained by integration of the flux density per beam over the whole source, is 66.9 ± 0.2 km s^{-1}. The line width of the (2, 2) and (3, 3) main HF lines, obtained by fitting a Gaussian profile to the line emission integrated over the whole source, are 8.2 ± 0.6 and 8.8 ± 0.4 km s^{-1}, respectively. Those obtained by integrating the line emission only over the core region (shown in Fig. 4) are 12.2 ± 1.2 and 11.6 ± 0.5 km s^{-1}, respectively. The average line width of the (2, 2) and (3, 3) satellite lines from the core region are 8.1 ± 0.9 and 9.0 ± 2.1 km s^{-1}, respectively.

Figure 6 shows a velocity-position contour diagram of the NH_3 emission in the (3, 3) transition, at 5.″3 × 3.″8 and 2.45 km s^{-1} resolution, made from a cut along an east-west direction at the declination of −19°52′19.″2. We identify two features in this plot. The most prominent one is a spatially compact (about ~3″ in size), broad velocity feature (~12 km s^{-1} wide), with a

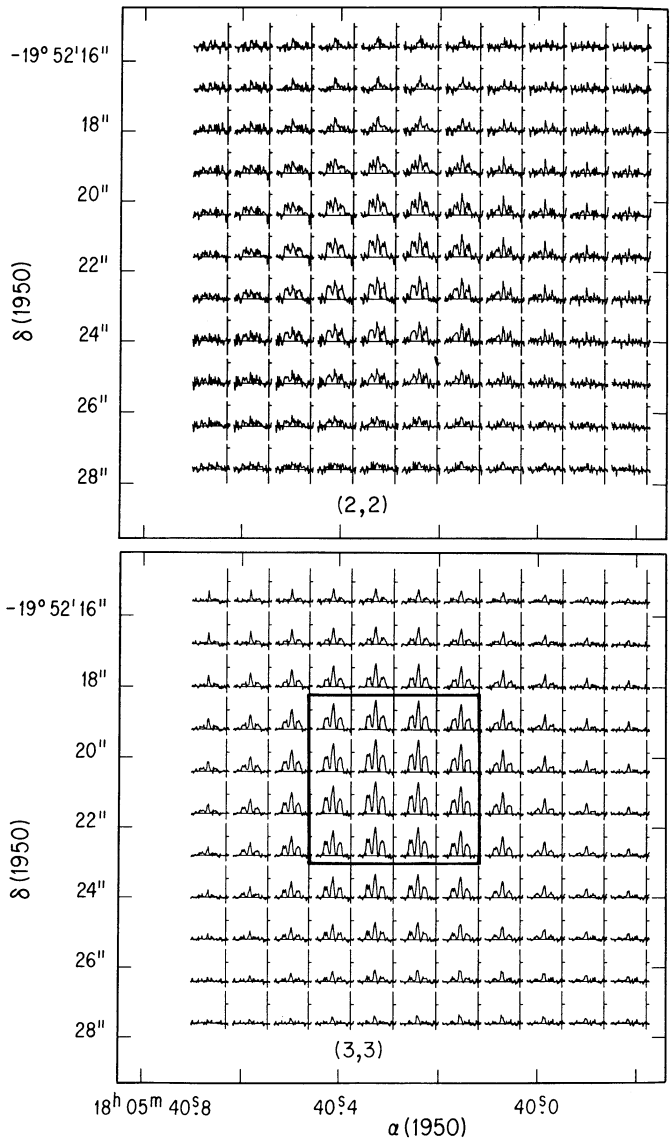

FIG. 4.—Beam-averaged profiles of the ammonia emission from the G10.47+0.03 cloud. *Top*: (2, 2) inversion transition. The velocity scales increases from −10.9 to 129.8 km s^{-1}, *right to left*. *Bottom*: (3, 3) inversion transition. The velocity increases from −10.5 to 129.3 km s^{-1}, *right to left*. The tick mark in the flux density per beam scale corresponds to a value of 0.5 Jy per beam. Spectra are at intervals of 1.″2.

central velocity of ~67 km s^{-1}. The four satellite HF components of this feature can be easily recognized at the velocities of ~38, 45, 88, and 96 km s^{-1}. The second feature that we identify is a diagonal, spatially extended and narrow in velocity, component. Its center velocity shifts by ~4.1 km s^{-1} over a region of ~15″. The HF satellite components of this feature are difficult to see, suggesting it has lower opacities than the compact component.

3.2.2. NH_3 *G10.46+0.03*

This ammonia cloud, located ~20″ east of the bright cometary region of ionized gas seen in the radio continuum map (see Fig. 1), is associated with the weak ultracompact H II region G10.46+0.03A (Wood & Churchwell 1989). Toward the NH_3 G10.46+0.03 cloud we detected the main HF lines of

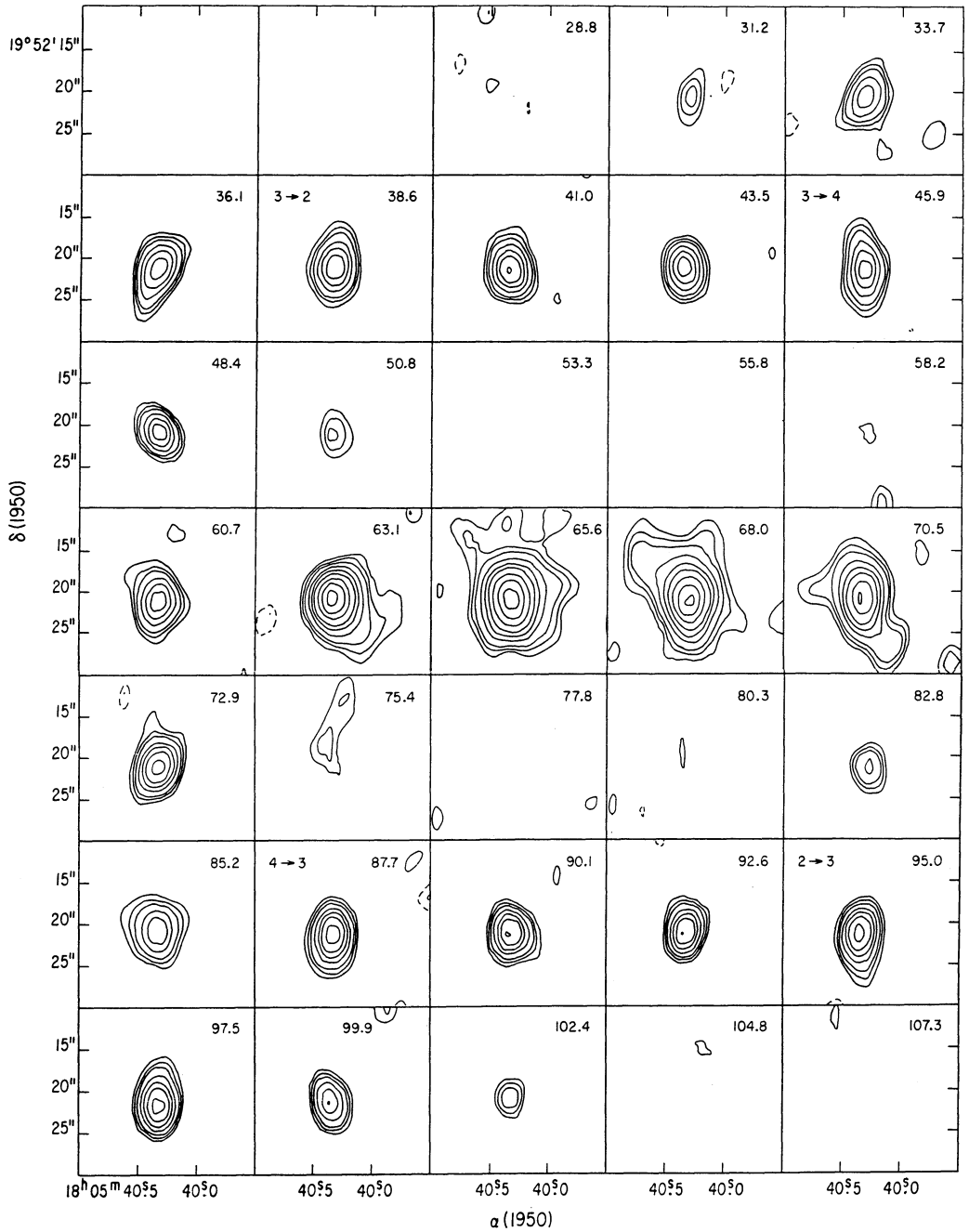

FIG. 5.—Line channel maps of the emission in the (3, 3) inversion transition of ammonia toward the NH_3 G10.47+0.03 cloud with 5".3 × 3".8 resolution. The LSR velocity of each map is indicated at the top right of the panel. Contour levels are {−4, −3, 3, 4, 5, 7, 9, 11, 14, 17, and 20} × 30 mJy per beam. The locations of the satellite hyperfine components, assuming an LSR velocity of 66.9 km s^{-1} for the main component, are indicated at the top left of the appropriate panels by their F′ → F values.

the (2, 2) and (3, 3) inversion transitions in emission. The satellite lines were undetected, indicating that the main line has an opacity of less than about 4. Upper (3 σ) limits for the flux densities per beam in the (2, 2) and (3, 3) satellite lines, determined from a map made adding all four line channel maps at the velocities expected for the satellite lines, are 87 mJy per beam and 42 mJy per beam, respectively.

The line profiles of the (3, 3) inversion transition of ammonia over an 16".8 × 15".6 region covering this source are shown in Figure 7. The pixel size is 1".2. The main HF line is clearly detected in emission while the satellite lines are undetected. The emission, with a peak brightness temperature of 19 ± 2 K, arises from a region of ~16" × 10" in size.

Spectra of the emission in the (2, 2) and (3, 3) main lines, integrated over the whole angular extent of the source, are shown in Figure 8. The center velocity and width of the (2, 2; m) line emission, determined by fitting a Gaussian profile to the spectra, are, respectively, 71.2 ± 0.3 and 3.4 ± 0.7 km s^{-1}. For the (3, 3; m) line emission we found a line center velocity of 71.4 ± 0.2 km s^{-1} and a line width of 3.6 ± 0.7 km s^{-1}. The

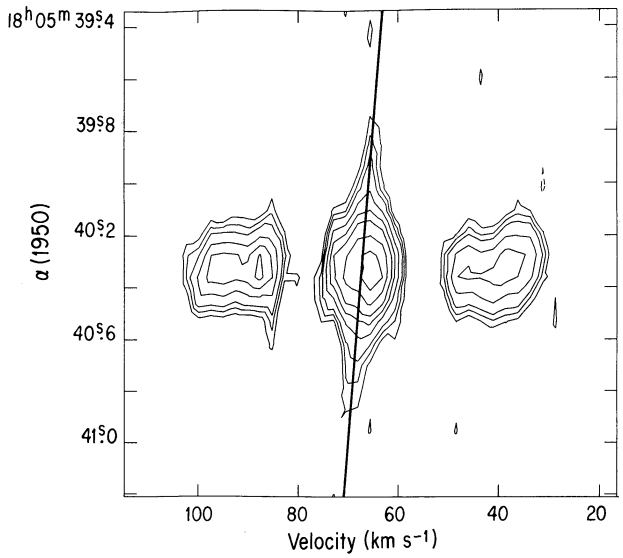

FIG. 6.—Velocity-position map of the NH_3 (3, 3) line emission, along an east-west line at $\delta(1950) = -19°52'19''.2$. The contour levels are $\{-3, 3, 4, 5, 7, 9, 11, 14, \text{and } 17\} \times 30$ mJy per beam. The angular resolution is $5''.3 \times 3''.8$.

flux densities at the center of the line, derived from the Gaussian fittings, are 1.82 ± 0.29 Jy for the (2, 2; m) line and 1.78 ± 0.23 Jy for the (3, 3; m) line.

Figure 9 shows a velocity-position contour map of the (3, 3) line emission, at $5''.3 \times 3''.8$ and 2.45 km s^{-1} resolution, made along an east-west direction at the declination of $-19°52'43''.2$. This plot exhibits an arc shaped structure, with the gas at the center of the arc being blueshifted, by ~ 2 km s^{-1}, with respect to the mean velocity of the gas near the outer edges of 72.6 km s^{-1}.

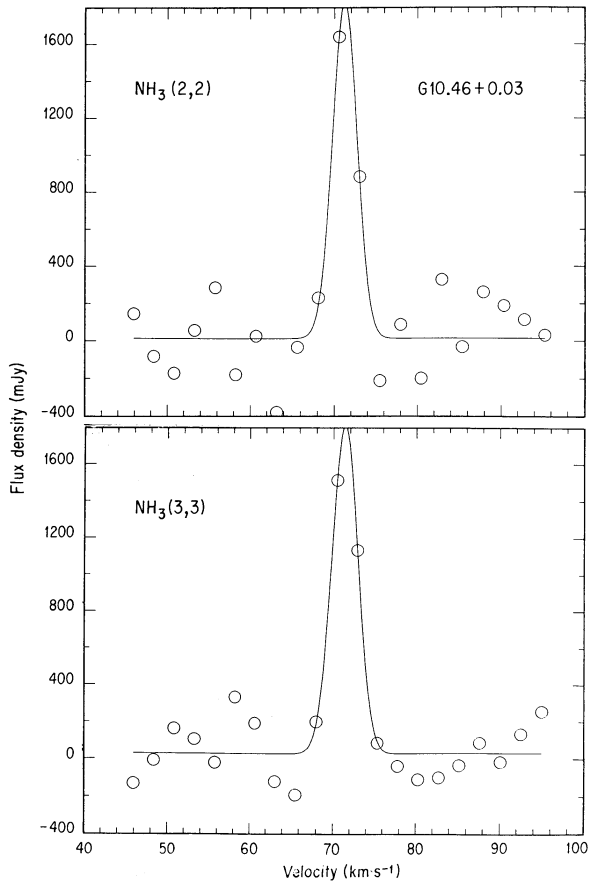

FIG. 8.—Integrated spectra of the NH_3 emission from the G10.46+0.03 cloud. *Top*: (2, 2) inversion transition. *Bottom*: (3, 3) inversion transition.

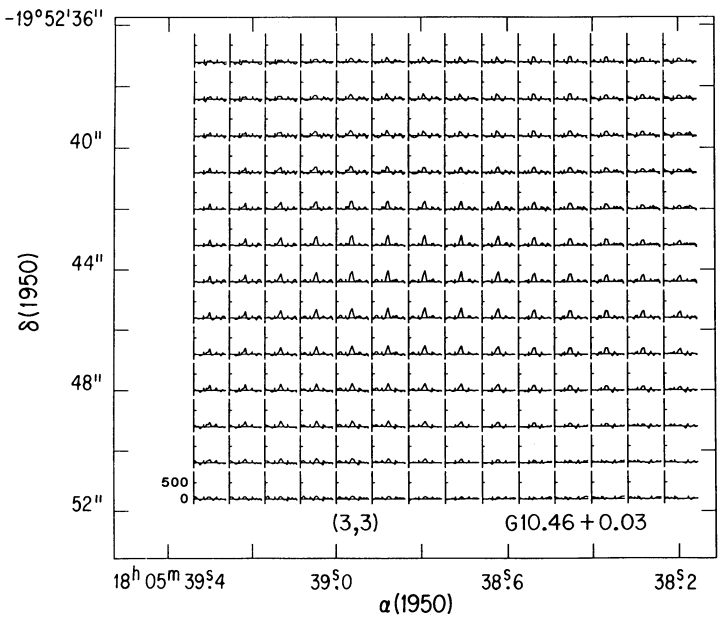

FIG. 7.—Beam-averaged profiles of the ammonia emission in the (3, 3) inversion transition from the G10.46+0.03 cloud. The velocity increases from -10.5 to 129.3 km s^{-1}, *right to left*.

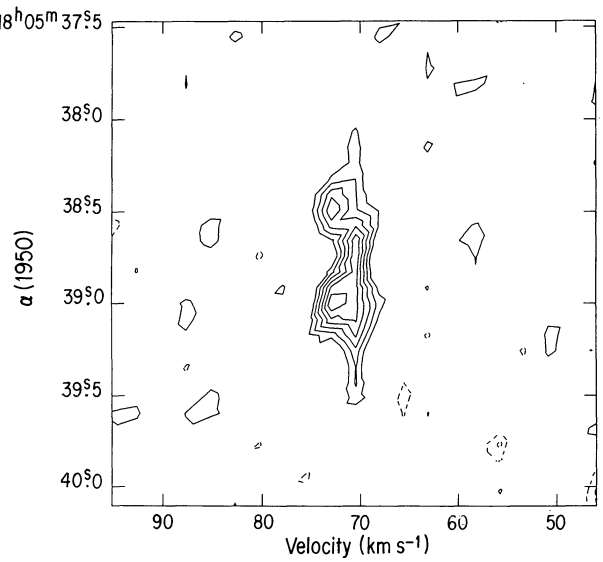

FIG. 9.—Velocity-position map of the NH_3 (3, 3) line emission from the NH_3 G10.46+0.03 cloud, along an east-west line at $\delta(1950) = -19°52'43''.2$. The contour levels are $\{-3, -2, 2, 3, 4, 5, 6, \text{and } 7\} \times 30$ mJy per beam. The angular resolution is 5".3 × 3".8.

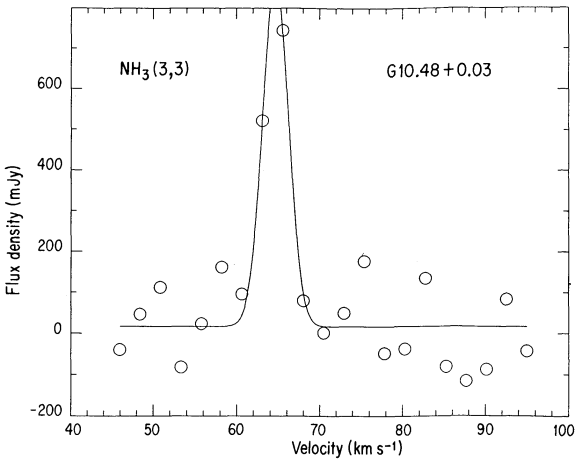

FIG. 10.—Integrated spectra of the NH_3 emission, in the (3, 3) inversion transition, from the G10.48+0.03 cloud.

3.2.3. NH_3 *G10.48+0.03*

Toward this cloud no radio continuum emission at 23.9 GHz was detected at a limit of 13 mJy. We detected ammonia emission in the main HF lines of the (2, 2) and (3, 3) inversion transitions. The satellite lines were below our detection limits. Upper (3 σ) limits for the flux densities per beam in the (2, 2) and (3, 3) satellite lines are 87 and 42 mJy per beam, respectively. The (3, 3; m) line emission, having a peak brightness temperature of 14 K, arises from a region of $\sim 14'' \times 6''$ in size.

Figure 10 shows the spectra of the (3, 3) transition, obtained by integration of the flux densities per beam over the whole extent of this source. The center velocity and width of the (3, 3; m) line emission, determined by fitting a Gaussian profile to the spectra, are 64.7 ± 0.2 km s^{-1} and 3.6 ± 0.8 km s^{-1}, respectively. Line channel maps of the emission in the (3, 3) inversion transition of NH_3, in the velocity range from 60.7 to 70.5 km s^{-1}, are shown in Figure 11. The channel width is 2.45 km s^{-1}. At the velocity of 63.1 km s^{-1} the emission arises mainly from the edges of the molecular structure, while at 65.6 km s^{-1} the emission peaks near the center of the structure.

4. ANALYSIS AND DISCUSSION

In the following analysis we derive physical parameters of the three ammonia clouds detected toward the $l = 10°.5$, $b = 0°.0$ Galactic region from our observations of the (2, 2) and (3, 3) inversion transition lines. For this purpose we have used the standard interpretation of the NH_3 spectra as described by Ho & Townes (1983). The derived parameters are summarized in Table 3. In addition, we discuss the kinematics of the ammonia structures and their relationship to the compact regions of ionized gas within that complex star forming region.

4.1. NH_3 *G10.47+0.03*

Toward this cloud we detected emission in all the hyperfine quadrupole components of both the (2, 2) and (3, 3) inversion transitions. Maps of the emission in the satellite and main lines of the (3, 3) inversion transition, shown in Figure 12, suggest that the G10.47+0.03 ammonia cloud has a core-halo structure. The emission from the HF satellite lines, which presumably samples a hotter and denser molecular component, arises from a compact region of $\sim 3''.9 \times 2''.3$ in size, hereafter called the core, that is embedded in a larger, $\sim 10''.2 \times 7''.8$, region delineated by the emission in the main line, hereafter called the halo. To derive physical parameters of the core structure, we integrated the NH_3 line emission over the $4''.8 \times 4''.8$ region shown in Figure 4.

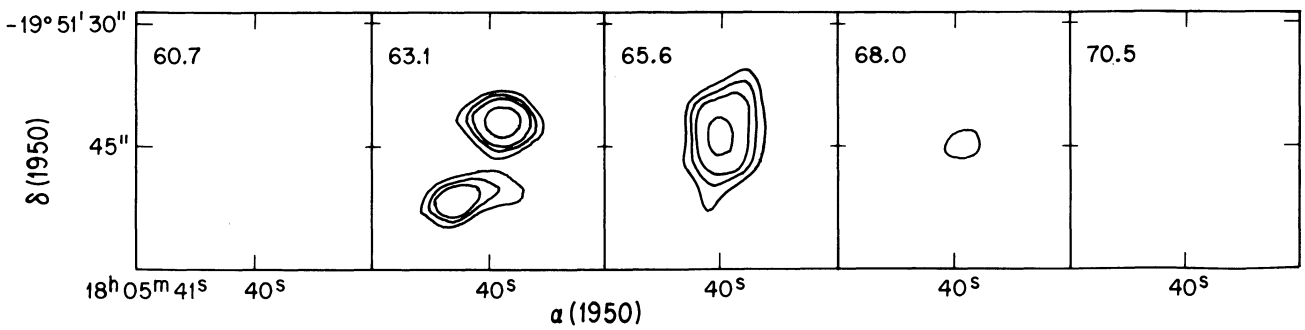

FIG. 11.—Line channel maps of the (3, 3) ammonia emission toward the NH_3 G10.48+0.03 cloud with 6".0 resolution. The LSR velocity is indicated in the top left. Contour levels are $\{-3, 3, 4, 5, \text{and } 7\} \times 30$ mJy per beam.

TABLE 3

DERIVED PARAMETERS OF THE AMMONIA STRUCTURES

Source	L (pc)	T_{rot} (K)	$N(NH_3)$ (cm^{-2})	$n(H_2)$[a] (cm^{-3})	$M(H_2)$ ($M_\odot$)
G10.47+0.03:					
Core	0.08	75	3.2×10^{18}	1.2×10^{7}	210
Halo	0.25	35	4.3×10^{17}	5.6×10^{5}	260
G10.46+0.03	0.36	48	1.3×10^{16}	1.2×10^{4}	28
G10.48+0.03	0.25	47	9.0×10^{15}	1.2×10^{4}	14

[a] Assuming an $[H_2/NH_3]$ abundance ratio of 10^6.

Optical depths.—The detection of the main and satellite HF lines of a given inversion transition allows a direct estimate of its total optical depth. In order to make opacity maps we made a new set of line maps, with a synthesized beam size of 6″.0 × 6″.0, to further increase the sensitivity to low surface brightness emission. Since the satellite lines have approximately the same relative intensities, we averaged all four satellite lines, in order to improve the signal-to-noise ratio, before calculating the opacities. In generating the opacity maps the data in the main and satellite line maps were clipped at their 3 σ noise level. Figure 13 shows maps of the opacities of the (2, 2, m) and (3, 3; m) lines, computed from the ratio of the brightness temperature in the line maps of the main and satellite components assuming equal beam-filling factors and equal values of the excitation temperatures. The optical depth of the (3, 3; m) line increases from ~8 at the edge of the compact region to ~27 at its central position; that of the (2, 2; m) line increases from ~4 to ~20. Using the unsmoothed data we find peak optical

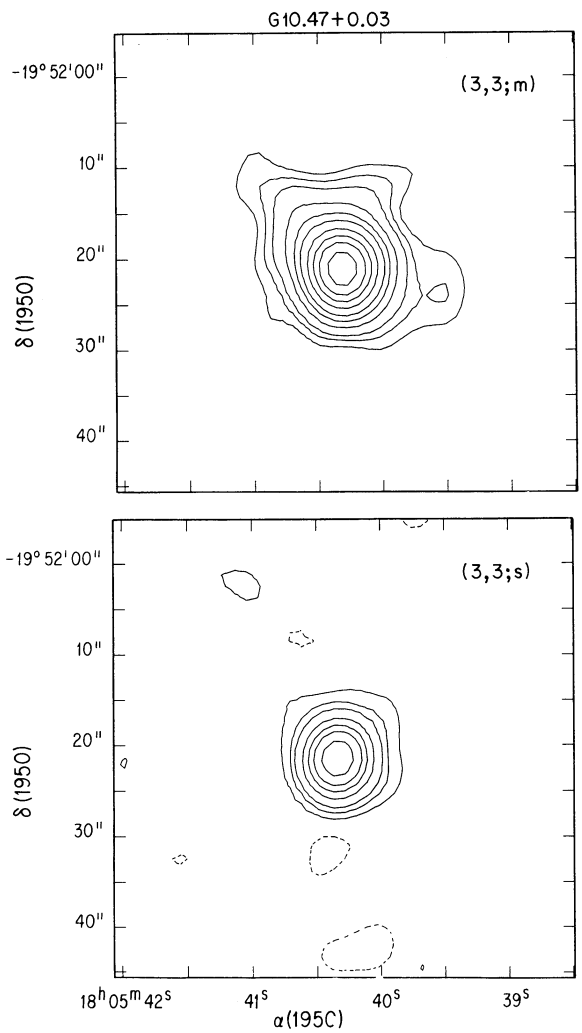

FIG. 12.—Contour maps of the NH_3 emission in the (3, 3) inversion transition, from the G10.47+0.03 molecular cloud. *Top*: main-line emission. Contour levels are {−3, 3, 4, 5, 7, 9, 11, 14, 17, 20, and 24} × 30 mJy per beam. *Bottom*: satellite line emission. Contour levels are {−1, 1, 2, 3, 5, 7, 9, and 12} × 30 mJy per beam.

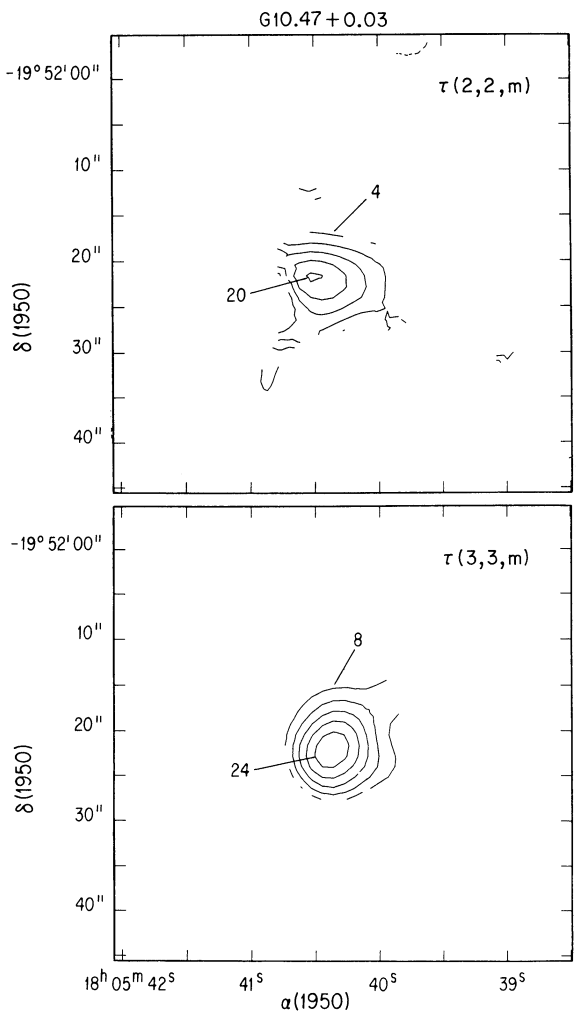

FIG. 13.—Contour maps of NH_3 optical depths toward G10.47+0.03. *Top*: optical depth of the (2, 2) main HF line. Contour levels are {−4, 4, 8, 12, 16, and 20}. *Bottom*: optical depth of the (3, 3) main HF line. Contour levels are {−4, 4, 8, 12, 16, 20, and 24}.

depths in the (2, 2; m) and (3, 3; m) lines of 25 and 37, respectively. These optical depths are among the largest so far derived for molecular cores associated with compact H II regions. The corresponding opacities in the satellite lines are 1.6 and 1.1 for the (2, 2) and (3, 3) transitions.

Rotational temperature.—The rotational temperature between the (2, 2) and (3, 3) levels can be derived from the ratio of their optical depths. Using the maps of the optical depths in the main lines (see Fig. 13) we made a map of the rotational temperature assuming equal excitation temperatures for the (2, 2) and (3, 3) levels. Figure 14 shows a cut of this map made passing through the peak position, at $\alpha = 18^h05^m40^s.32$ and $\delta = 19°52'22''.2$, and along a direction with a position angle of 67° east of north. We note that implicit in this derivation is the assumption of uniform conditions along a line of sight; hence, these values of the rotational temperature should be taken only as an average value along the line of sight. The rotational temperature, T_{rot}, increases from $\sim$25 K at the edge of the molecular structure to $\sim$70 K at the center of the core. Using the unsmoothed data we found a peak T_{rot} of 79 K. A comparison of this temperature with the observed peak beam averaged brightness temperature, of 69 K, suggests that the molecular gas in the central position covers a large fraction of the beam area.

Two of the three ultracompact H II regions in the line of sight toward this cloud are projected right at the peak position of the ammonia rotational temperature map, suggesting that they are the source of heating of the molecular gas. A minimum least-squares fit to a power-law relation between T_{rot} and the projected distance from the exciting stars, p gives

$$T_{rot}(p) = 72\left(\frac{p}{10^{17}\ \mathrm{cm}}\right)^{-0.4\pm0.1}\ \mathrm{K}\ , \qquad (1)$$

for p in the range between 1×10^{17} and 7×10^{17} cm. A determination of the dependence of T_{rot} with the distance from the central stars, r, requires to simulate spectral line images of three dimensional molecular clouds (see Keto 1990), a task beyond the scope of this paper. We note, however, that in the presence of temperature gradients, due to the dependence of the population level density with temperature ($\propto \exp^{-E/kT}/T^{5/2}$), the main contribution to the opacity arises from the hotter gas in the line of sight. If T_{rot} decreases monotonically with r we then expect, to a first approximation, that $T_{rot}(p) \sim T_{rot}(r)$. Relation (1) is in good agreement with that predicted by a model in which the heating of NH_3 is provided by collisions with warm grains which are in turn heated by the stellar emission from the embedded central sources that excite the H II regions (Scoville & Kwan 1976).

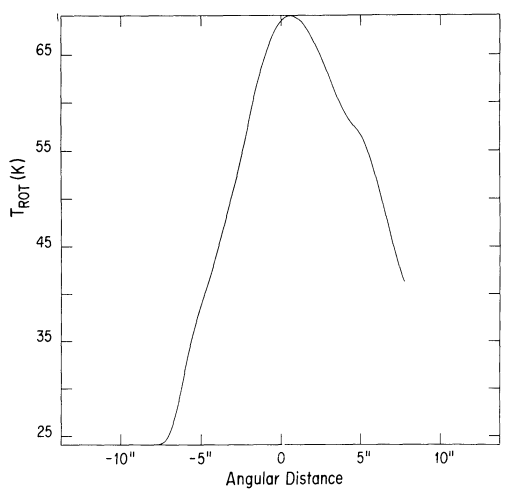

FIG. 14.—Line profile of the rotational temperature, between the (2, 2) and (3, 3) transitions of NH_3, toward the G10.47+0.03 cloud along a direction with a position angle of 67° east of north.

Column densities and molecular masses.—The total column density of NH_3 can be computed knowing the optical depth, the rotational temperature, and the excitation temperature of an inversion transition (cf. eq. [8]) of Garay & Rodríguez 1990). Assuming that the excitation temperature is equal to the rotational temperature, using $T_{rot} \approx 35$ K for the envelope and 75 K for the core region, we derive peak NH_3 column densities of $\sim 4 \times 10^{17}$ cm^{-2} and $\sim 3 \times 10^{18}$ cm^{-2}, respectively. The ammonia densities can be derived from the column densities dividing by a characteristic length. Adopting path lengths of 0.25 pc for the envelope and 0.084 pc for the core, which correspond to the geometrical mean of the observed projected sizes, we derive ammonia densities of 0.6 and 12 cm^{-3}, respectively.

The determination of the molecular hydrogen density requires to know the abundance ratio $[NH_3/H_2]$. This ratio has been estimated to be between 10^{-7} for small and dark clouds (Ungerechts, Walmsley, & Winnewiser 1980) and 10^{-5} in the dense nucleus of the Orion molecular cloud (Genzel et al. 1982). For the G10.47+0.03 cloud we will adopt a fractional abundance of 10^{-6}, as determined for other clouds with similar physical conditions (Henkel, Wilson, & Mauersberger 1987), implying H_2 densities of 5.6×10^5 and 1.2×10^7 cm^{-3} for the envelope and core regions, respectively. Recently, Cesaroni et al. (1991) reported observations of G10.47+0.03 in three lines of $C^{34}S$ made with angular resolutions ranging from 12″ to 26″. Using statistical equilibrium calculations they derive an H_2 density of 6.3×10^5 cm^{-3}, similar to the density that we derived for the halo region from the ammonia observations. Given the large uncertainties inherent to both derivations, for instance in the $[C^{34}S/H_2]$ and $[NH_3/H_2]$ abundance ratios or in the magnitude of the velocity gradients, the agreement is remarkable. Finally, assuming radii of 0.042 pc and 0.125 pc, we derive hydrogen molecular masses of $\sim$210 and $\sim$260 $M_\odot$ for the core and halo regions, respectively.

Line widths and kinematics.—The line widths of the G10.47+0.03 cloud are significantly broader than the average line width of a large sample of ammonia sources associated with ultracompact H II regions, of $\sim$3 km s^{-1} (Churchwell et al. 1990). Even though the latter line width, derived from observations with 40″ angular resolution, may be dominated by emission from cold gas surrounding the warm compact molecular cores, the significantly larger line width of the warm G10.47+0.03 ammonia cloud cannot be solely explained by either its high kinetic temperature or by its large optical depth. Most likely, the large line widths are due to the presence of greater ordered or turbulent gas motions.

From the position-velocity contour plot of the (3, 3) transition made at a position angle of 0°, shown in Figure 6, we have identified two structures: (1) a spatially compact, broad-velocity feature seen in all five HF components; and (2) a diagonal feature, more extended spatially but narrower in velocity, seen clearly only in the main HF line. We interpret this last feature as the signature of approximate rigid body rotation of the gas in the optically thin envelope of the G10.47+0.03 molecular cloud. The change in the center veloc-

ity across the envelope, of 4.1 ± 0.5 km s^{-1} over a length scale of 0.43 pc, implies a velocity gradient of 9.5 ± 1.1 km s^{-1} pc^{-1}. The mass required to gravitationally bind the rotational motions is $\sim 180\ M_\odot$. Using a rather uncertain value for the $[NH_3/H_2]$ abundance ratio of 10^{-6}, we previously estimated a molecular mass for the G10.47+0.03 ammonia cloud of $\sim 470\ M_\odot$. In addition, there are at least two B0 and one B0.5 ZAMS stars ionizing the region (Wood & Churchwell 1989), contributing $\sim 60\ M_\odot$ (Allen 1973). This brings our estimate of the total mass in this region up to $\sim 530\ M_\odot$. Consequently, we conclude that there is sufficient mass within the G10.47+0.03 cloud to gravitationally bind the rotational motion of the molecular envelope.

We now turn to the discussion of the origin of the broad line widths observed in the core region. Thermal broadening is too small to explain the observed line widths; even at the high kinetic temperature of the core, 75 K, the thermal width is only ~ 0.5 km s^{-1}. Saturation broadening, given the values of the opacities derived for the core region (see § 4.1), is also negligible for the satellites lines but is expected to become important for the main lines. We note that the line widths measured toward the core in the main lines are greater, by ~ 3 km s^{-1}, than those observed in the satellite lines. The difference in line widths can be ascribed to saturation effects in the main lines. The broadening observed in the satellite lines, of ~ 9 km s^{-1}, requires, however, an additional explanation. Possible mechanisms involve the presence of either rotational, infalling, or outflowing gas motions. If the gas in the core is roughly freely falling toward the central stars, the mass needed to produce an infall velocity of ~ 4.5 km s^{-1} (about one-half of the line width) at the core radius of 0.042 pc is $\sim 100\ M_\odot$. Unless the supporting mechanisms against gravitational collapse (magnetic fields, rotation, etc.) have been lost only recently, a serious difficulty with this model is that the collapse time of the core is very short, $\sim 10^4$ yr, compared with the time scale of formation of the luminous early-type B stars at the center of the flow ($\sim 10^5$ yr). Thus, we consider this possibility the least likely.

The second possibility we examine is that the molecular gas in the core is spiralling toward the compact H II regions, slowly falling but rapidly spinning up due to partial conservation of the angular momentum. In a simple analysis (cf. Ho & Haschick 1986) the velocity gradient scales as R^{-2} if the angular momentum is conserved. Given that the velocity gradient is 9.5 ± 1.1 km s^{-1} pc^{-1} at a scale of ~ 0.21 pc, we expect a gradient of ~ 240 km s^{-1} pc^{-1} at 0.042 pc. When observed with our low angular resolution these rotational motions should produce a line width of ~ 10 km s^{-1} [$\sim(\Delta v/\Delta R) \times R$], in good agreement with the observed value. If this hypothesis is correct, we may conclude that a significant fraction of the initial angular momentum is still left at scales of ~ 0.05 pc. A drawback of this model is that in the velocity-position diagram shown in Figure 6 we do see a broad, nearly circular structure, while the model predicts that a broad but diagonal structure should be observed.

The third possibility is that the core gas is undergoing outflow motions, such as those proposed in the case of G5.89−0.39 by Gómez et al. (1991). The outflow motions could be driven by the expansion of the hot ionized gas around the newly formed stars. The hot ammonia gas would then be part of the heated and compressed region behind the shock front around a compact H II region. With the angular resolution provided by the present observations we cannot discern among the different possibilities discussed above. Clearly, observations with higher angular and spectral resolution are needed to resolve the structure of the motions across the core.

4.2. NH_3 *G10.46+0.03*

Toward the G10.46+0.03 cloud we detected emission in the main HF line of the (2, 2) and (3, 3) inversion transitions, but not in the satellite lines. From the observed values and upper limits of the flux densities per beam integrated over the whole source, we derive upper limits of 0.5 and 0.9 for the opacities in the main line of the (2, 2) and (3, 3) transitions, respectively.

Assuming that the emission in the main lines is optically thin, the ratio of flux densities in the (2, 2; m) and (3, 3; m) lines [$S_L(2, 2; \mathrm{m}) = 1.82 \pm 0.29$; $S_L(3, 3; \mathrm{m}) = 1.78 \pm 0.23$ Jy] implies a rotational temperature for the G10.46+0.03 cloud of 48 ± 6 K. An estimate of the optical depth can then be obtained from the observed brightness temperature of the line, T_L, and the rotational temperature, $T_{\rm rot}$, using the relation $T_L = (T_{\rm rot} - T_{\rm bg})(1 - e^{-\tau})$, which assumes that the filling factor of the emitting region is equal to 1 and that the excitation temperature of the line is equal to $T_{\rm rot}$. Using the observed value of $T_L(3, 3; \mathrm{m}) = 19 \pm 2$ K, $T_{\rm rot} = 48$ K, and $T_{\rm bg} = 3$ K, we find $\tau(3, 3; \mathrm{m}) \sim 0.6$. From this opacity and the line width of the (3, 3; m) line, of 3.6 km s^{-1}, we derive a total column density for the ammonia of $N(NH_3) \simeq 1.3 \times 10^{16}$ cm^{-2}.

Since the NH_3 lines are optically thin, the mass of molecular gas can be derived from the parameters observed in one transition. In terms of the flux density and line width of the (3, 3; m) line, the total mass of molecular gas is given by

$$M(\mathrm{H_2}) = 2.4 \times f(T_{\rm ex}, T_{\rm rot}) \left(\frac{D}{\mathrm{kpc}}\right)^2 \left(\frac{[\mathrm{H_2/NH_3}]}{10^6}\right) \times \left(\frac{\Delta v}{\mathrm{km\ s^{-1}}}\right) \left[\frac{S_L(3, 3; \mathrm{m})}{\mathrm{Jy}}\right] M_\odot\ , \quad (2)$$

where

$$f(T_{\rm ex}, T_{\rm rot}) = \left(\frac{T_{\rm rot}}{100\ \mathrm{K}}\right)^{3/2} \left(\frac{T_{\rm ex}}{100\ \mathrm{K}}\right) \times \frac{\exp\,(124.5/T_{\rm rot})}{\{1/[\exp\,(h\nu_{33}/kT_{\rm ex}) - 1] - 1/[\exp\,(h\nu_{33}/kT_{\rm bg}) - 1]\}}\ .$$

Using $T_{\rm ex} = T_{\rm rot} = 48$ K, and assuming an $[H_2/NH_3]$ abundance ratio of 10^6, we derive a molecular mass for G10.46+0.03 of $28\ M_\odot$.

Turning now our discussion to the dynamics of this cloud, we interpret the arc-shaped structure seen in Figure 9 as indicating expansion motions of a shell of molecular gas. Toward the center of the shell the expansion is along the line of sight and therefore we see blueshifted gas. At the edges of the shell, the gas is moving perpendicular to the line of sight and the observed radial velocity is the mean velocity of the system. The expansion velocity, determined as the difference between the average radial velocity of the gas at the center and in the outer regions of the arc structure, is 2.0 ± 0.5 km s^{-1}.

4.3. NH_3 *G10.48+0.03*

Toward the G10.48+0.03 cloud we detected emission only in the main line of the (2 2) and (3) inversion transitions. We derive upper limits for the opacities in the (2, 2) and (3, 3) main lines of 0.9 and 1.1, respectively.

Following the same line of reasoning applied to derive the

physical parameters of the G10.46+0.03 cloud, we find that the G10.48+0.03 cloud has a rotational temperature of 47 ± 6 K, an optical depth in the (3, 3 m) line of 0.4, and an NH_3 column density of 9×10^{15} cm^{-2}. Further, adopting a path length in the line of sight of 0.24 pc, we derive an H_2 molecular density of 1.2×10^4 cm^{-3}. The molecular mass of this cloud, derived from equation (2) assuming an $[H_2/NH_3]$ abundance ratio of 10^6, is 14 $M_\odot$.

An examination of the emission in the individual line channel maps of the (3, 3) transition (see Fig. 11) suggests that this source is undergoing radial motions. At the velocity of 63.1 km s^{-1} the emission arises mainly from the edges of the molecular structure, while at 65.6 km s^{-1} the emission peaks near the center of the structure. Although the signal-to-noise ratio is low, the observed velocity structure suggests a radial flow with a velocity of 1.2 ± 0.6 km s^{-1}. It is not possible, however, to determine whether we are observing the front hemisphere of an infalling structure or the back hemisphere of an outflowing structure. The mass required to generate an infall velocity of 1.2 km s^{-1} at the radius of 0.12 pc is 20 $M_\odot$, which is about equal to the mass estimated from the ammonia measurements. The observed radial flow is thus consistent with gravitational collapse. Since this cloud does not appear to have a significant source of internal energy, it may represent a molecular condensation undergoing collapse in the earliest stage of star formation.

5. SUMMARY

We mapped, with the VLA at an angular resolution of $\sim 4''$, the ammonia emission in the $(J, K) = (2, 2)$ and (3, 3) inversion transitions, toward the Galactic star-forming region at $l = 10\overset{\circ}{.}5$, $b = 0\overset{\circ}{.}0$. The main results and conclusions presented in this paper are summarized as follows.

1. We detected three distinct compact ammonia clouds, in a region of $\sim 2'$ in diameter, at the Galactic coordinates of $l = 10\overset{\circ}{.}47$, $b = 0\overset{\circ}{.}03$; $l = 10\overset{\circ}{.}46$, $b = 0\overset{\circ}{.}03$; and $l = 10\overset{\circ}{.}48$, $b = 0\overset{\circ}{.}03$.

2. The brightest ammonia cloud, having a peak brightness temperature of 69 K in the (3, 3) main line, is associated with the G10.47+0.03 cluster of compact H II regions. It exhibits a core-halo structure. The emission in the HF main line of the (3, 3) inversion transition arises from a $\sim 10\overset{''}{.}2 \times 7\overset{''}{.}8$ structure, elongated in a direction oriented $\sim 36°$ east of north. The emission from the HF satellite lines, which presumably sample denser and hotter gas, arises from a region of $\sim 3''$ in size near the center of the envelope.

2.1. The rotational temperature increases from ~ 25 K in the outer edge of the envelope (radius of 0.2 pc) to ~ 75 K in the central region of the core, scaling outward with radius as $r^{-0.4}$. The ultracompact H II regions located at the center of the core are the most probable source of heating of the molecular gas. The column density of NH_3 increases from $\sim 4 \times 10^{17}$ cm^{-2} in the envelope to $\sim 3 \times 10^{18}$ cm^{-2} in the core. We derive H_2 densities of 6×10^5 and 1×10^7 cm^{-3} and molecular masses of 260 and 210 $M_\odot$ for the halo and core regions, respectively.

2.2. The molecular envelope appears to be slowly rotating. Velocity-position maps show that the line center velocity steadily shifts by ~ 4.1 km s^{-1} over a region of ~ 0.43 pc. The corresponding velocity gradient is 9.5 ± 1.1 km s^{-1} pc^{-1}. The mass required to gravitationally bind the rotational motions is ~ 180 $M_\odot$.

2.3. The NH_3 emission from the core region exhibits remarkably broad line widths, of ~ 12 km s^{-1} in the main lines and ~ 9 km s^{-1} in the satellite lines. The broad line widths may be explained as due to either spiraling motions of a gas in the core that is slowly collapsing toward the central compact H II regions while conserving most of its angular momentum, or due to outflowing motions driven by the expansion of the H II region. The difference in line widths between the main and satellite lines may be ascribed to saturation effects in the former.

3. The NH_3 G10.46+0.03 cloud, having a velocity of 71.3 km s^{-1}, is associated with the ultracompact H II region G10.46+0.03A. It has a size of ~ 0.36 pc, a peak rotational temperature of 48 K, and a peak NH_3 column density of 1×10^{16} cm^{-2}. We derive an H_2 density of 1.2×10^4 cm^{-3} and a total mass of 28 $M_\odot$. The velocity structure suggests that this cloud is expanding with a velocity of ~ 2 km s^{-1}.

4. The NH_3 G10.48+0.03 cloud, having a line center velocity of 65.4 km s^{-1}, does not appear to be associated with a significant source of internal energy. At 23.9 GHz we did not detect radio continuum emission at a flux density level of 13 mJy. It has a peak rotational temperature of 47 K and an NH_3 column density of 9×10^{15}cm^{-2}. The molecular mass is 14 $M_\odot$. The observed velocity structure is consistent with infall generated by the self-gravity of a 20 $M_\odot$ object.

G. G. acknowledges support from an Henri Chrétien Award and from the Smithsonian Institution of Washington. This research has been partially supported by the Chilean FONDECYT under grant 0907/92.

REFERENCES

Allen, C. W. 1973, Astrophysical Quantities (London: Athlone)
Braz, M. A., & Sivagnanam, P. 1987, A&A, 181, 19
Cesaroni, R., Walmsley, C. M., & Churchwell, E. 1992, A&A, 256, 618
Cesaroni, R., Walmsley, C. M., Kömpe, C., & Churchwell, E. 1991, A&A, 252, 278
Churchwell, E., Walmsley, C. M., & Cesaroni, R. 1990, A&AS, 83, 119
Garay, G., & Rodríguez, L. F. 1990, ApJ, 362, 191
Garay, G., Rodríguez, L. F., Moran, J. M., & Churchwell, E. 1993, ApJ, in press (GRMC)
Genzel, R., & Downes, D. 1977, A&AS, 30, 145
Genzel, R., Downes, D., Ho, P. T. P., & Bieging, J. 1982, ApJ, 259, L103
Gómez, Y., Rodríguez, L. F., Garay, G., & Moran, J. M. 1991, ApJ, 377, 519
Henkel, C., Wilson, T. L., & Mauersberger, R. 1987, A&A, 182, 137
Ho, P. T. P., & Haschick, A. D. 1986, ApJ, 304, 501
Ho, P. T. P., & Townes, C. H. 1983, ARA&A, 21, 239
Keto, E. R. 1990, ApJ, 355, 190
Keto, E. R., Ho, P. T. P., & Haschick, A. D. 1987a, ApJ, 318, 712
Keto, E. R., Ho, P. T. P., & Reid, M. J. 1987b, ApJ, 323, L117
Scoville, N., & Kwan, J. 1976, ApJ, 206, 718
Ungerechts, H., Walmsley, C. M., & Winnewiser, G. 1980, A&A, 88, 259
Wood, D. O. S., & Churchwell, E. 1989, ApJS, 69, 831 (WC)